

Article

The Low Strain Rate Response of As-Cast Ti-6Al-4V Alloy with an Initial Coarse Lamellar Structure

Zhixiong Zhang ¹ , Shoujiang Qu ¹, Aihan Feng ¹, Xin Hu ² and Jun Shen ^{1,*} ¹ School of Materials Science and Engineering, Tongji University, Shanghai 201804, China;

zhangzx8963@126.com (Z.Z.); qushoujiang@tongji.edu.cn (S.Q.); aihanfeng@tongji.edu.cn (A.F.)

² Sicuan Shifang Future Aerospace Industry LLC, Shifang 618400, China; huxinbuaa@163.com

* Correspondence: junshen@tongji.edu.cn; Tel.: +86-21-6958-1009

Received: 28 March 2018; Accepted: 12 April 2018; Published: 15 April 2018



Abstract: The microstructure and microtexture evolution of the as-cast Ti-6Al-4V alloy with an initial lamellar microstructure was investigated in the temperature range of 900–1050 °C and the low strain rate range of 10^{-3} – 10^{-1} s⁻¹. In the ranges 900–950 °C and 10^{-3} – 10^{-2} s⁻¹, globularization of the α lamellar structure took place; the initial α {0001} texture softened, and the {0001} texture rotated to the transverse direction. Additionally, the increasing strain rate led to more randomization. The globularization process was considered to be continuous dynamic recrystallization (CDRX). At strain rates higher than 10^{-2} s⁻¹ and temperatures between 900 and 950 °C, flow instabilities occurred. In the β range, dynamic recrystallization (DRX) occurred at a temperature of 1050 °C and a strain rate of 10^{-3} s⁻¹.

Keywords: Ti-6Al-4V; globularization; texture; lamellar structure; DRX

1. Introduction

The Ti-6Al-4V is one of the most important and widely used $\alpha + \beta$ titanium alloys in the world [1–3]. Bulk metalworking of Ti-6Al-4V alloy is generally comprised of a series of mechanical processing steps that are used to transform the as-cast microstructure into an equiaxed $\alpha + \beta$ two-phase microstructure [4]. Previous studies [5,6] have shown that thermomechanical processing (TMP) of the Ti-6Al-4V alloy above the β transus temperature results in a lamellar microstructure morphology that consists of α platelets and an inter-platelet β phase. When processed below the β transus, the conversion of transformed β microstructure to the equiaxed microstructure needs superior process control to avoid the generation of the microstructure defects like flow localization or wedge cracks [7,8]. Expect for processing temperature, other thermomechanical parameters, such as strain rate and strain, also influence the microstructure [9–12]. The response of the lamellar microstructure during hot deformation will be of great importance in projecting industrial thermomechanical processing schedules to get the desired microstructure without defect occurrence.

Besides the microstructure, the texture is more critical to the mechanical properties of the Ti-6Al-4V alloy [13]. In spite of the great importance of crystallographic textures, the information about the microtexture development of Ti-6Al-4V alloy deformed in low strain rate ranges is still limited.

The objective of this study is to determine the microstructure and microtexture evolution of the as-cast Ti-6Al-4V with a coarse lamellar structure in low strain rate ranges, and to systematically investigate the hot deformation behavior in both $\alpha + \beta$ and β phase fields.

2. Materials and Methods

2.1. Materials

The ELI grade Ti-6Al-4V alloy used in this work is in cylinder form with a diameter of 355 mm produced by conventional ingot metallurgy. Its chemical composition is shown in Table 1. The β transus temperature reported for this grade was about 975 °C [4].

Table 1. Chemical composition of ELI grade Ti-6Al-4V alloy (wt. %).

Al	V	Fe	Ti	Si	C	O	N	H
6.08	4.03	0.14	Bal.	0.013	0.018	0.11	0.0047	0.0008

2.2. Experimental Procedures

Cylindrical compression samples of 8 mm diameter and 12 mm height were machined from the as received cylinder. Hot compression tests were performed in the temperature range of 900–1050 °C at 50 °C intervals and constant true strain rates (10^{-3} , 5×10^{-3} , 10^{-2} , 5×10^{-2} , 10^{-1} s^{-1}) on a Gleeble-3800 simulator with a height reduction of 60% (Figure 1). The temperature of the specimens was monitored by a chromel-alumel thermocouple welded on the middle of the surface of the specimens. Two tantalum foils with a thickness of 0.1 mm were put between the anvil and the specimen to minimize the friction. Prior to isothermal compression, specimens were heated to the designed temperature with a speed of 10 °C/s and held for 5 min to obtain a homogeneous heat distribution. After compression, each specimen was water quenched immediately. Hot deformed samples were axially sectioned parallel to the compression axis and the longitudinal sections were prepared in order to determine the microstructure evolution.

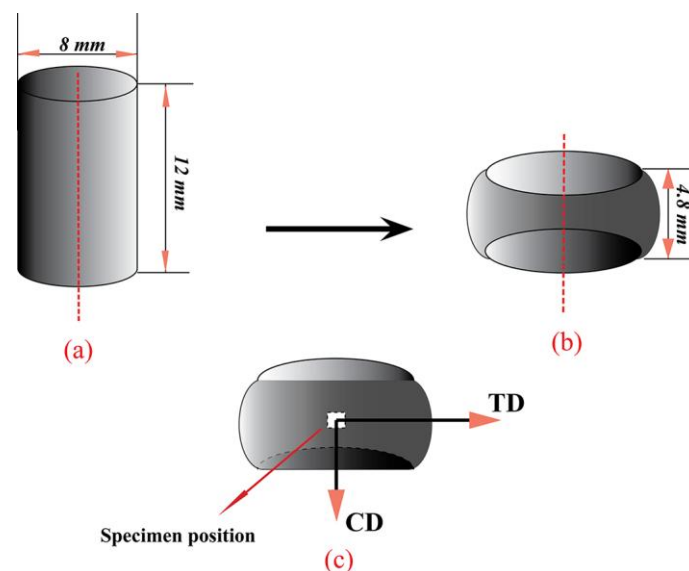


Figure 1. Schematic of isothermal compression and viewing position (CD and TD represents compressing direction and transverse direction, respectively): (a) undeformed sample; (b) deformed sample; (c) sample position.

The microstructures of the deformed samples were examined using optical microscopy (OM, Carl Zeiss Axio Observer. 5 m, Jena, Germany), scanning electron microscope (SEM, FEI Quanta 250, Houston, TX, USA), transmission electron microscopy (TEM, Hitachi H-800, Tokyo, Japan), and electron backscatter diffraction (EBSD, Apollo 300, Cambridge, UK). The specimens were electrochemically

polished with a solution of 60% carbinol, 34% *n*-butanol, and 6% perchloric acid using a voltage of 30 V and a current of 80 mA for the OM, SEM, and EBSD characterization. The TEM foils were twin-jet electrochemical polished in a solution of 60% carbinol, 4% perchloric acid, and 36% *n*-butanol. The EBSD characterizations were performed with an increment step of 0.2 μm . In order to remove the orientation noise and uncertainty caused by severe deformation, misorientation below 2° was not taken into account. Low angle grain boundaries (LAGBs) were defined as the grain boundaries with misorientation between 2° and 15° and shown in yellow. High angle grain boundaries (HAGBs) were defined as those with misorientation above 15° and shown in black.

3. Results

The initial microstructure was lamellar and had Widmannstatten morphology (Figures 2 and 3). It consisted of large prior β grains of about 6–7 mm separated by a grain boundary α layer of 5 μm thick. The α lamellar colonies formed inside the prior β grains, and α lamellae, which formed on the prior β grain boundaries, maintained a Burger's relationship with their parent β matrix [14–16]. The thickness of the α lamellae was about 3 μm , and a continuous β layer of approximately 1 μm thick was distributed in between the grain boundary α and the Widmannstatten sides-plates. As shown in Figure 3c,d), the texture of the scanned area consisted of two components. The stronger one can be expressed by Euler angles as ($\varphi_1 = 132^\circ$, $\Phi = 75^\circ$, $\varphi_2 = 38^\circ$), which is represented by A in the pole figures. Additionally, the weaker one is represented by B and can be expressed by Euler angles as ($\varphi_1 = 38^\circ$, $\Phi = 75^\circ$, $\varphi_2 = 10^\circ$). The textures all rotated approximately 75° from ND toward TD (ND represents the normal direction).

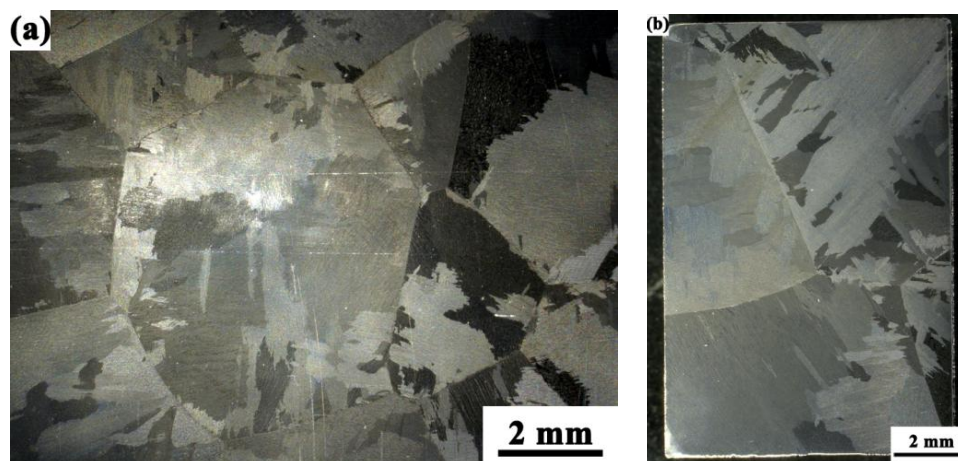


Figure 2. Macro structure of the undeformed sample: (a) top surface and (b) transverse section.

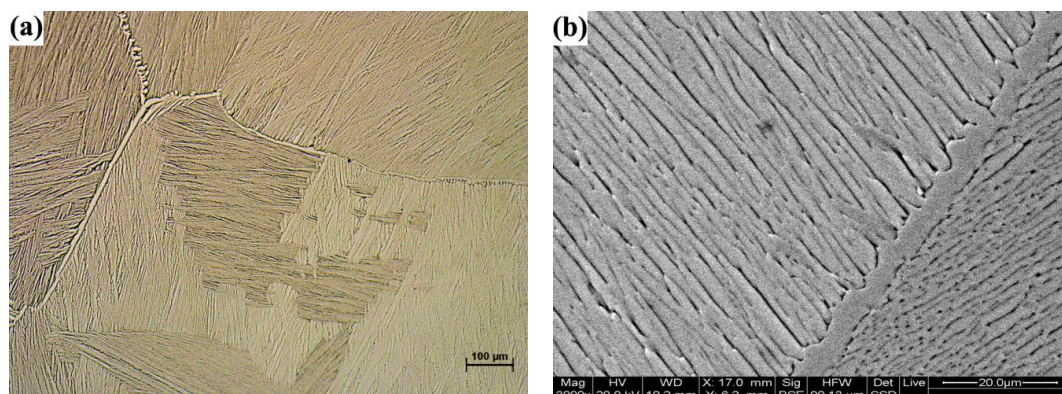


Figure 3. Cont.

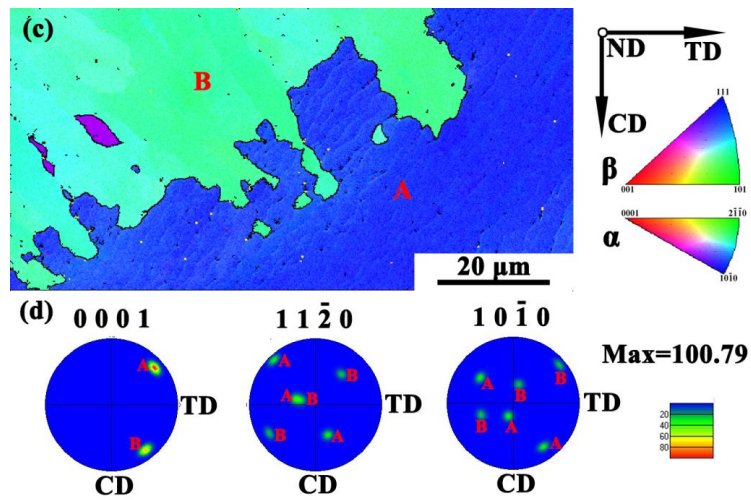


Figure 3. Initial microstructure of Ti-6Al-4V used in this study: (a) OM; (b) SEM; (c) the orientation map; and (d) pole figure.

Typical macro pictures of deformed specimen are shown in Figure 4. As shown in Figure 4, in the range of 10^{-3} – 10^{-2} s^{-1} , deformation bands in the samples were not clear, while in the range of 10^{-2} – 10^{-1} s^{-1} , adiabatic shear bands were obvious.

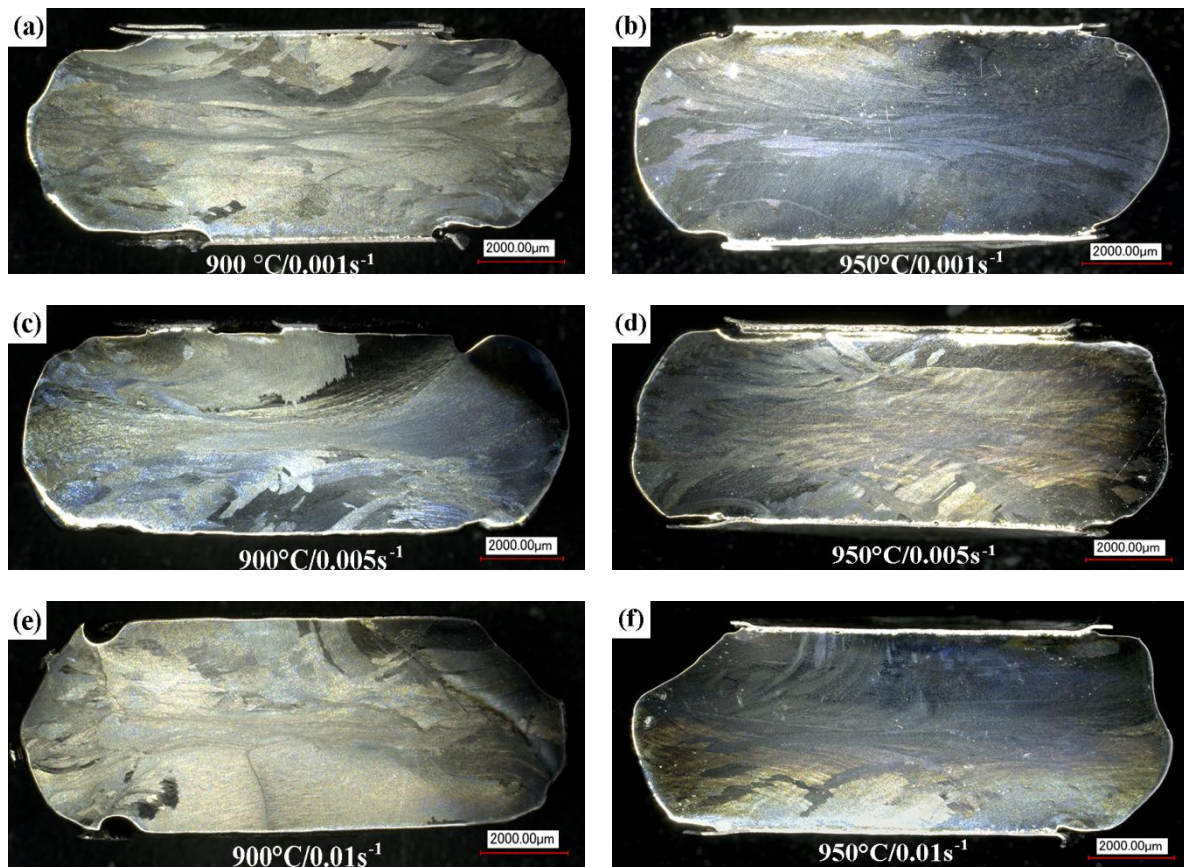


Figure 4. Cont.

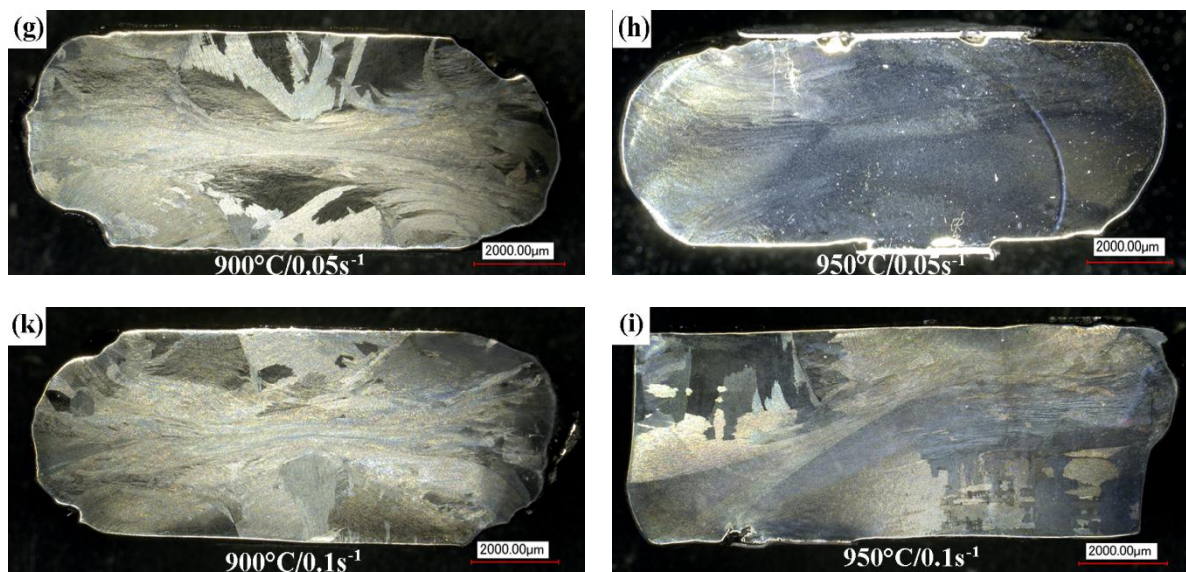


Figure 4. Macro pictures of Ti-6Al-4V sample deformed at (a) $900\text{ }^{\circ}\text{C}/10^{-3}\text{ s}^{-1}$; (b) $950\text{ }^{\circ}\text{C}/10^{-3}\text{ s}^{-1}$; (c) $900\text{ }^{\circ}\text{C}/5 \times 10^{-3}\text{ s}^{-1}$; (d) $950\text{ }^{\circ}\text{C}/5 \times 10^{-3}\text{ s}^{-1}$; (e) $900\text{ }^{\circ}\text{C}/10^{-2}\text{ s}^{-1}$; (f) $950\text{ }^{\circ}\text{C}/10^{-2}\text{ s}^{-1}$; (g) $900\text{ }^{\circ}\text{C}/5 \times 10^{-2}\text{ s}^{-1}$; (h) $950\text{ }^{\circ}\text{C}/5 \times 10^{-2}\text{ s}^{-1}$; (k) $900\text{ }^{\circ}\text{C}/10^{-1}\text{ s}^{-1}$; and (i) $950\text{ }^{\circ}\text{C}/10^{-1}\text{ s}^{-1}$.

Figure 5a–d,f exhibits different microstructures at various positions of Ti-6Al-4V sample compressed at a temperature of $900\text{ }^{\circ}\text{C}$ and a strain rate of 10^{-2} s^{-1} . According to Figure 5, three different deformation zones could be defined: “dead” zone at bottom and top areas near the contact surfaces, partial plastic deformation zone close to the both sides, and severe plastic deformation zone in the center. In this study, the microstructures of inner severe plastic deformation zone are determined.

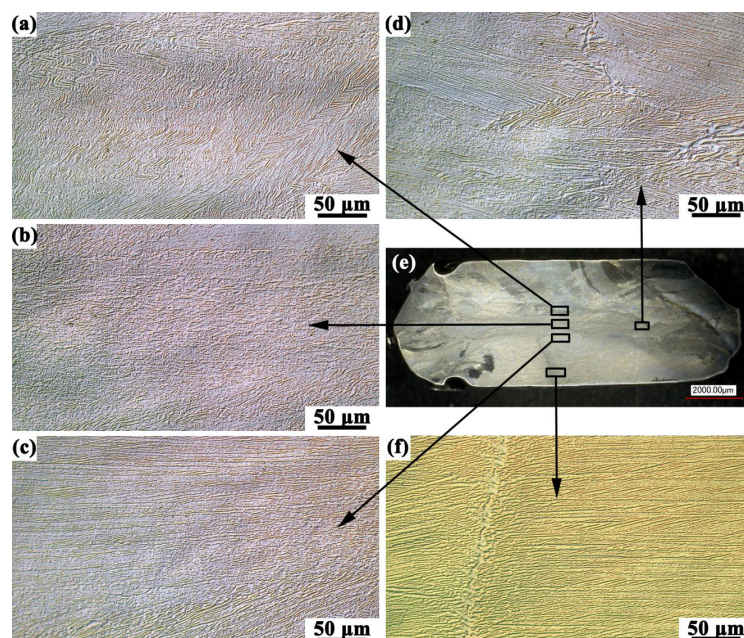


Figure 5. Macro picture of Ti-6Al-4V sample deformed at $900\text{ }^{\circ}\text{C}$ and a strain rate of 10^{-2} s^{-1} . (a,c,d) partial plastic deformation zone; (b) severe plastic deformation zone; (f) “dead” zone.

Microstructure of the samples deformed in the $\alpha + \beta$ phase field are shown in Figures 6 and 7. The studied areas were all taken from the central part of the deformed samples due to the largest

amount of deformation. From Figure 6, it is noted that the lower temperature and lower strain rate domain ($900\text{--}950\text{ }^{\circ}\text{C}$, $10^{-3}\text{--}10^{-2}\text{ s}^{-1}$) represented spheroidization of lamellar structure.

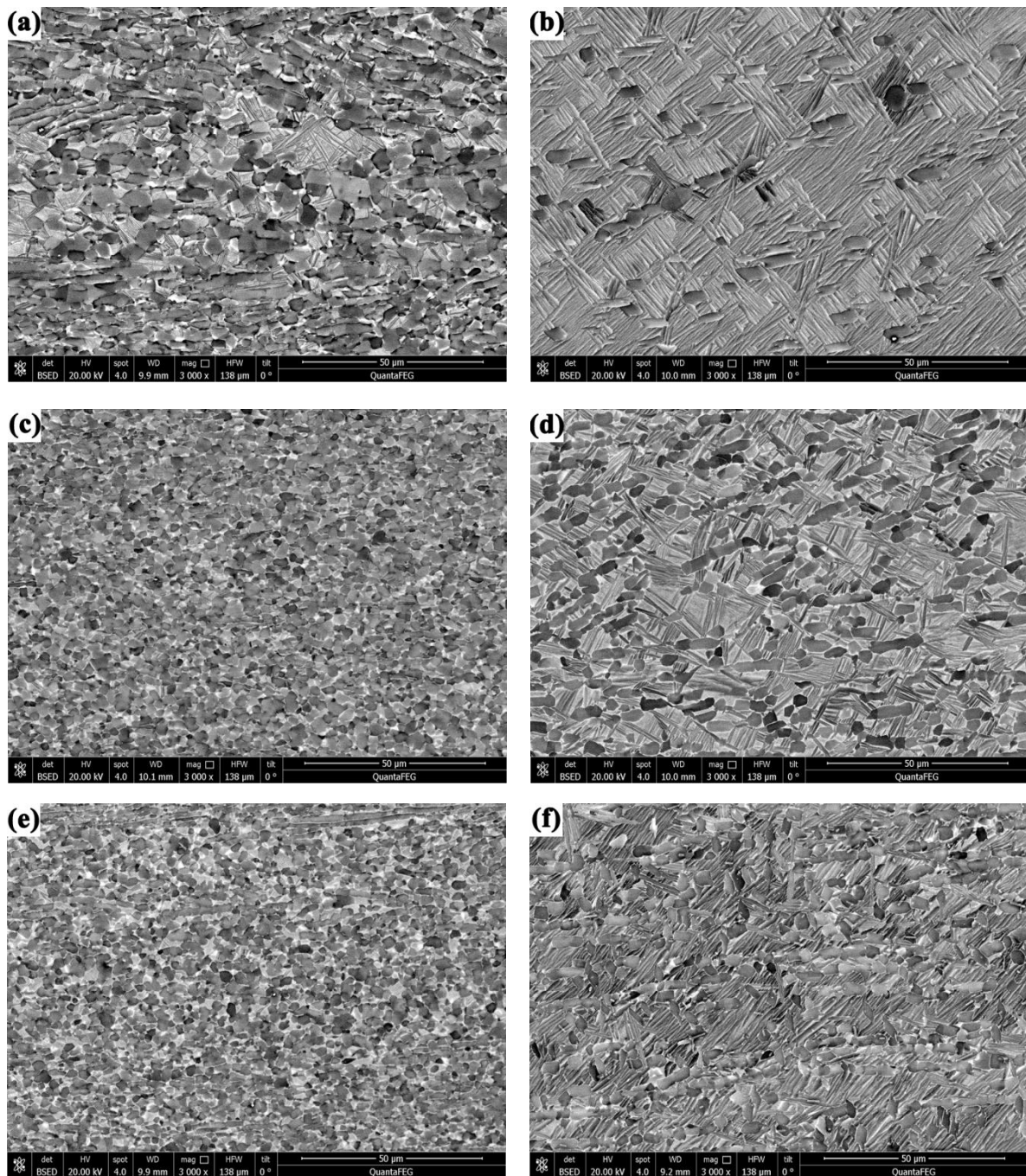


Figure 6. Microstructures of Ti-6Al-4V specimens deformed at (a) $900\text{ }^{\circ}\text{C}/10^{-3}\text{ s}^{-1}$; (b) $950\text{ }^{\circ}\text{C}/10^{-3}\text{ s}^{-1}$; (c) $900\text{ }^{\circ}\text{C}/5 \times 10^{-3}\text{ s}^{-1}$; (d) $950\text{ }^{\circ}\text{C}/5 \times 10^{-3}\text{ s}^{-1}$; (e) $900\text{ }^{\circ}\text{C}/10^{-2}\text{ s}^{-1}$; and (f) $950\text{ }^{\circ}\text{C}/10^{-2}\text{ s}^{-1}$.

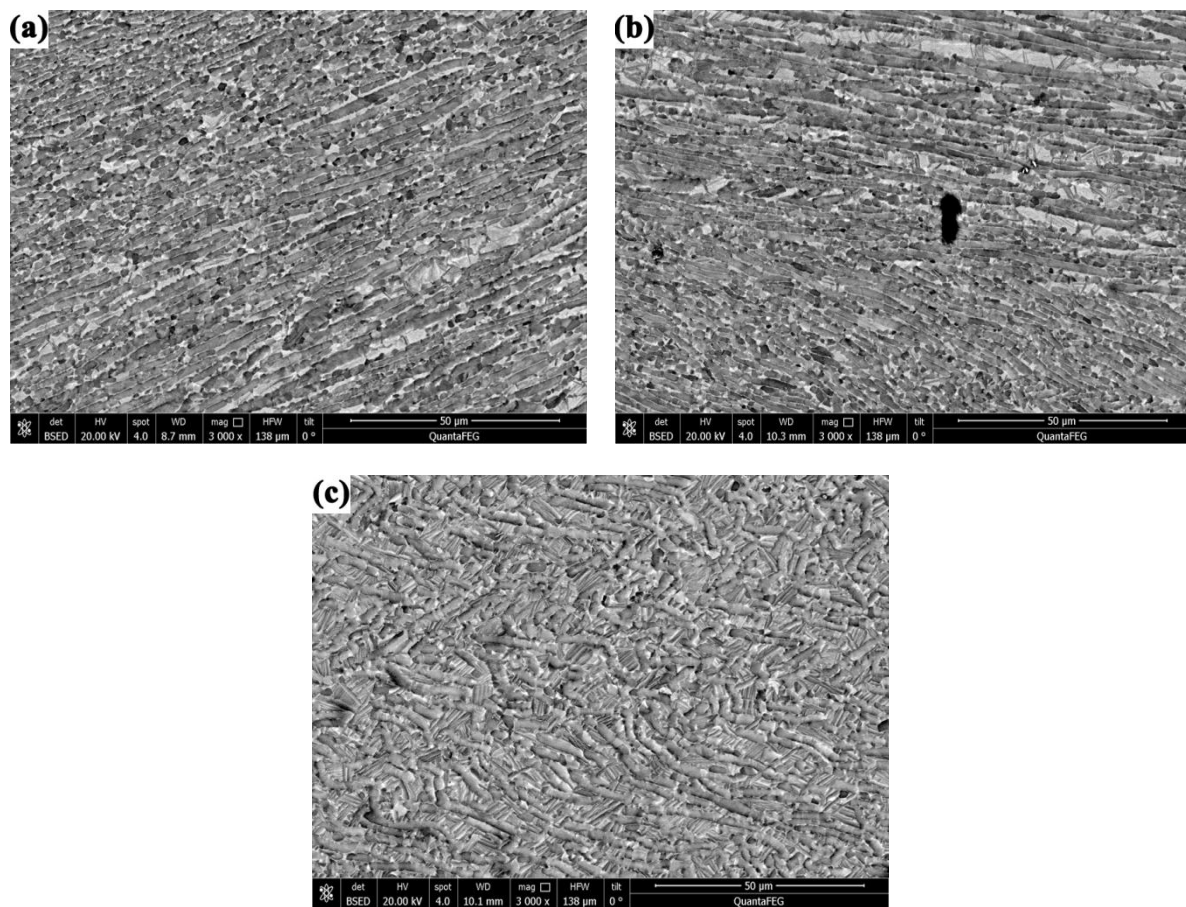


Figure 7. Microstructures of Ti-6Al-4V specimens deformed at (a) $900\text{ }^{\circ}\text{C}/5 \times 10^{-2}\text{ s}^{-1}$; (b) $900\text{ }^{\circ}\text{C}/10^{-1}\text{ s}^{-1}$; and (c) $950\text{ }^{\circ}\text{C}/10^{-1}\text{ s}^{-1}$.

Microstructural and microtexture evolution during the spheroidization process were further elucidated by EBSD and TEM. As shown in Figure 8, the microtexture of the specimen deformed at the temperature of $900\text{ }^{\circ}\text{C}$ and strain rate of 10^{-3} s^{-1} consisted of two components: one was the $\{0001\}$ transverse texture and the other was the $\{0001\}$ texture rotated 75° from ND to TD.

When deformed at a temperature of $900\text{ }^{\circ}\text{C}$ and strain rate of 10^{-2} s^{-1} , the microtexture of the specimen consisted of three components: there was an additional 50° $\{0001\}$ texture, except for the transverse texture and the 75° texture (Figure 9).

TEM images exhibited the detailed information of the globularization of α lamellae (Figures 10 and 11). As shown in Figure 10a,b, shearing of the α lamellae and splitting of α/α boundaries were observed, and formation of subgrains was observed inside the α phase (Figure 10c,d).

The microstructure of the samples deformed in the β phase field are shown in Figure 12; the results indicated that DRX occurred when the deformation temperature was in the β phase field.

As given in Figure 11, the penetration of the β phase along the α platelets was observed.

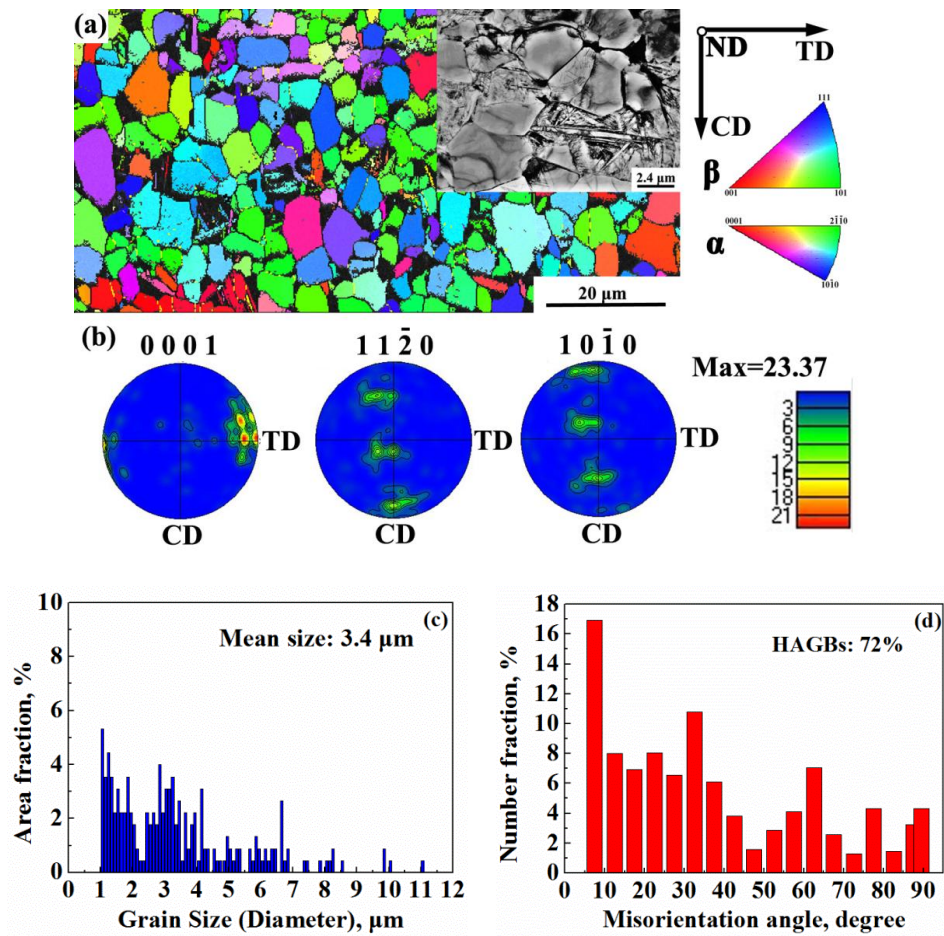


Figure 8. Microstructure and microtexture of Ti-6Al-4V specimens deformed at 900 °C/10⁻³ s⁻¹: (a) the orientation map; (b) pole figure; (c) distribution of grain size of α phase; and (d) grain boundary misorientation of α phase.

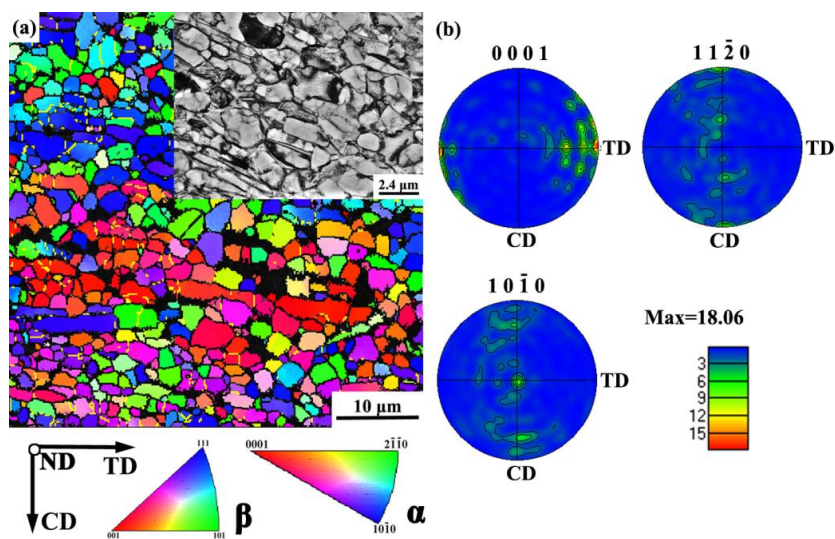


Figure 9. Cont.

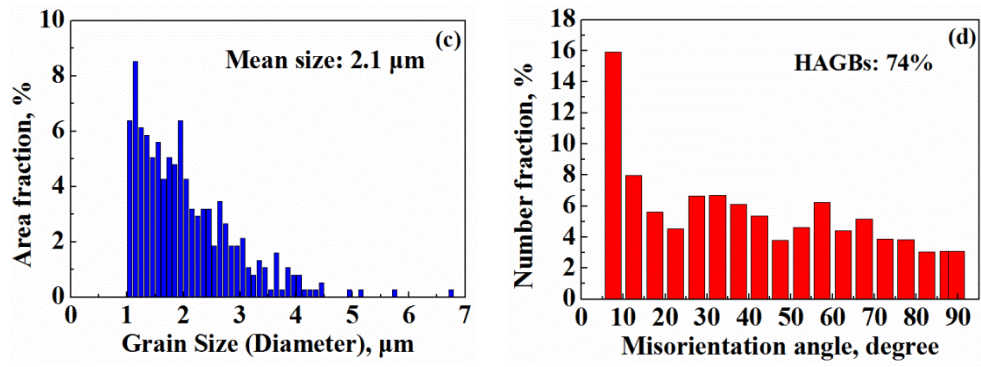


Figure 9. Microstructure and microtexture of Ti-6Al-4V specimens deformed at $900\text{ }^{\circ}\text{C}/10^{-2}\text{ s}^{-1}$: (a) the orientation map; (b) pole figure; (c) distribution of grain size of α phase; and (d) grain boundary misorientation of α phase.

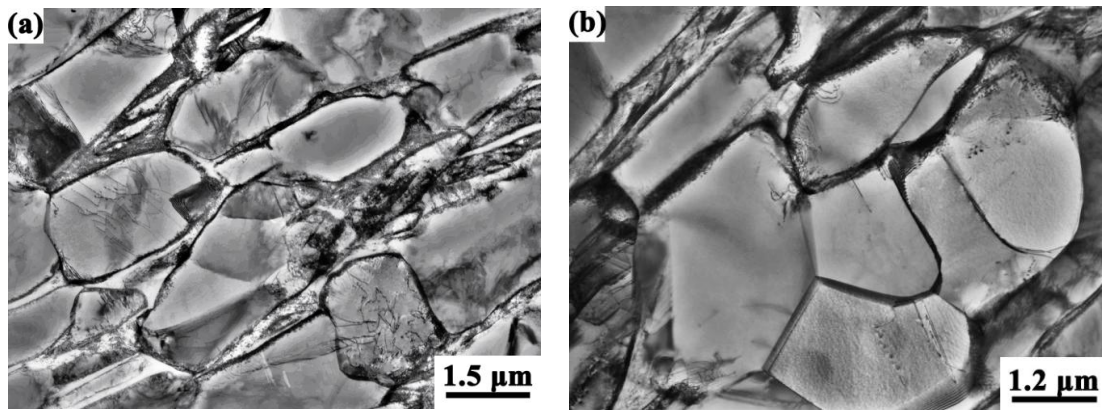


Figure 10. TEM images of Ti-6Al-4V specimens deformed at $900\text{ }^{\circ}\text{C}/10^{-3}\text{ s}^{-1}$: (a) breakdown of the lamellar structure and (b) subgrains inside the recrystallized grains.

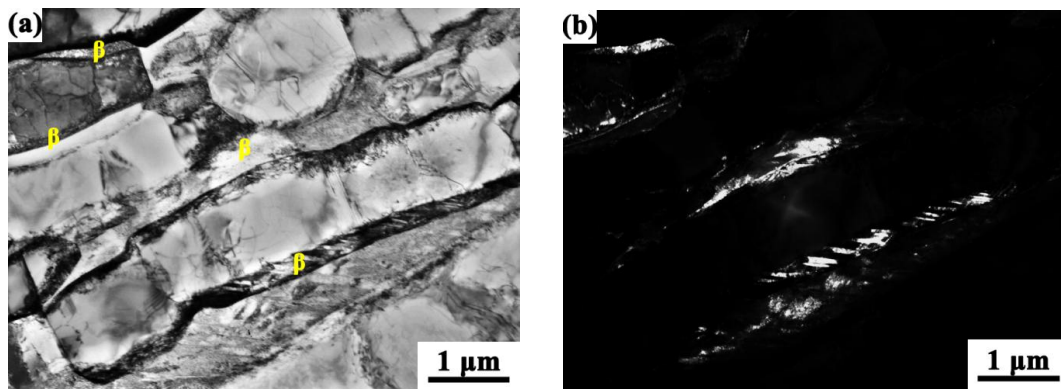


Figure 11. *Cont.*

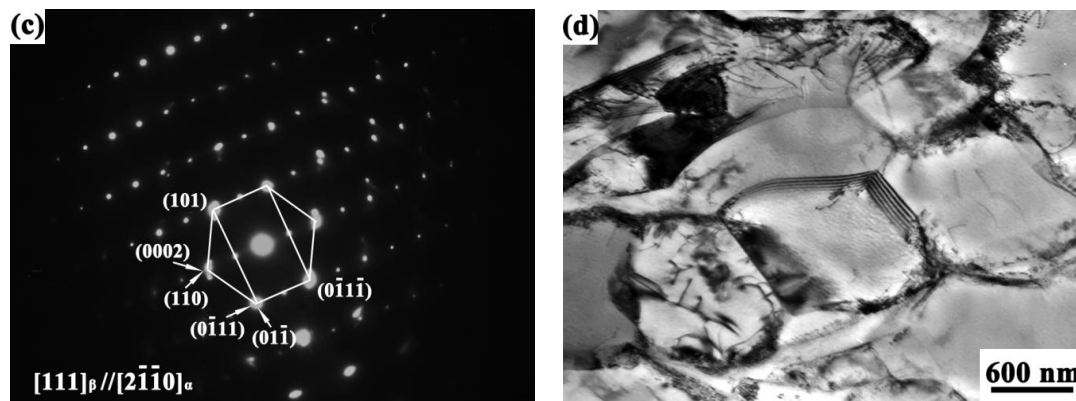


Figure 11. TEM images of Ti-6Al-4V specimens deformed at $900\text{ }^{\circ}\text{C}/10^{-2}\text{ s}^{-1}$: (a) bright field image; (b) dark field image; (c) SAED patterns; and (d) DRX grains.

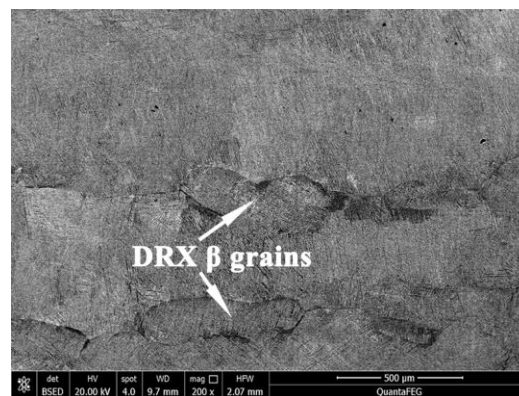


Figure 12. Microstructures of Ti-6Al-4V specimens deformed at $1050\text{ }^{\circ}\text{C}/10^{-3}\text{ s}^{-1}$.

4. Discussion

4.1. Globularization

In the ranges $900\text{--}950\text{ }^{\circ}\text{C}$ and $10^{-3}\text{--}10^{-2}\text{ s}^{-1}$, the microstructures of deformed samples exhibited the transformation of the lamellar structure of α phase to equiaxed. As seen in Figures 6, 8 and 9, microstructure of specimens compressed at $900\text{--}950\text{ }^{\circ}\text{C}$ and different strain rates indicated globularization of the α lamellar structure. It is shown that at $900\text{ }^{\circ}\text{C}$ large deformation broke down the α lamellae into segments; then, the small α segments transformed into spheroidized α_p particles, and the retained thin layers of β separated the α_p particles in a microstructure called fully equiaxed. The grain size of the primary α phase was $3.4\text{ }\mu\text{m}$ at a strain rate of 10^{-3} s^{-1} , and it reduced to $2.1\text{ }\mu\text{m}$, with the strain rate increasing to 10^{-2} s^{-1} (Figures 8 and 9).

The initial β grains and α colonies were completely lost during the deformation. The 75° texture was generally preserved from the as-received material, suggesting a degree of texture memory. And, the existence of transverse texture indicated the texture randomization resulting from the globularization process. Furthermore, the appearance of additional 50° texture suggested that the strain rate increase led to more randomization. The evolution of pole figure density also confirmed this conclusion.

In Figures 8 and 9, the LAGBs and HAGBs were represented by solid yellow lines and black lines, respectively. The fraction of HAGBs was high, and nearly all the new equiaxed grains were encircled by high-angle boundaries. On the contrary, low-angle boundaries mostly appeared in the retained lamellar α phase. Several works [8,17–21] on Ti-6Al-4V had provided insight into the globularization

process of the lamellar α phase during hot deformation. Weiss et al. [21] invoked the intense shear bands inside the α lamellae as the main driving force of the α breakdown, and boundaries were formed by β penetrating the α platelets by diffusion. Additionally, the observations agreed with this (Figure 11). Seshacharyulu [8,22] reported that the shearing of α lamellae was due to imposed shear strain; then, dislocations were generated along the line of shear, and an interface consisting of dislocations with same sign was formed; finally, the process of globularization of α phase was completed by migration of interfaces. Zherebtsov [23] also noted that dislocation walls formed in some of the lamellar α phases after a height strain ε of 0.29 and a microstructure involving a high dislocation density and subgrains were formed after strain ε of 0.69, and a mixed globular/lamellar microstructure was formed when the strain ε increased to 1.2. As given in Figures 10 and 11, the process of globularization could be considered as a type of CDRX. In this process, the low-angle boundaries formed by dislocations were produced at low strains, and then the LAGBs transformed into HAGBs at large strains to complete the globularization of α phase. Additionally, the fraction of the HAGBs increased from 72% to 74%, with the strain rate increasing from 10^{-3} s^{-1} to 10^{-2} s^{-1} . It was noted that the degree of recrystallization was increased with the strain rate increasing.

When the temperature was up to $950 \text{ }^\circ\text{C}$, the increasing temperature enabled the transformation of the β phase into new α lamellae in a matrix of retained β . The microstructure consisted of spherodized primary α particles and new lamellae of secondary α in a matrix of retained β phase, which was called a bimodal microstructure. The volume fraction of primary α phase increased with the strain rate increasing.

4.2. Deformation Behavior of the β Phase

DRX is an important microstructural mechanism that can occur during hot working of the Ti-6Al-4V alloy in the β phase field. As seen in Figure 12, microstructure of the specimen deformed at $1050 \text{ }^\circ\text{C}/10^{-3} \text{ s}^{-1}$ in the β phase field revealed that the new prior β grains were formed. Additionally, when deformed in the β phase field, the microstructure was comprised of almost complete martensite due to water quenching. This evidence clearly indicated that β phase underwent DRX.

4.3. Flow Instabilities

The microstructural observations in the temperature range $900\text{--}950 \text{ }^\circ\text{C}$ and strain rate range $0.03\text{--}0.1 \text{ s}^{-1}$ confirmed the flow instabilities of the coarse lamellar structure. Microstructures of the samples deformed under conditions covered in this regime were given in Figure 7. From Figure 7, it could be seen that, in the lower temperature regime, nonuniform deformation led to regions of intense localized shear in which the lamellae broke up. So, the instability mechanism was mainly flow localization, even cracking. The explanation for this was that during deformation, the time was not sufficient for the heat generated during deformation to conduct away, which caused highly localized flow instability [10]. Otherwise, when deformed at $950 \text{ }^\circ\text{C}/10^{-1} \text{ s}^{-1}$, the majority of the α laths became kinked. Generally, kinks were formed inside colonies during deformation at low temperatures ($550\text{--}700 \text{ }^\circ\text{C}$) [24,25]. However, in severe deformation conditions, the adjacent colonies rotated towards one another, causing localized flow in the boundary between the colonies and therefore loss of the (orientation relationship) OR [26]. In details, α laths broke up with increasing strain, resulting in the formation of rows of shorten α grains/subgrains (Figure 7c). The instability domain identified above must be taken into consideration to avoid defect during hot deformation of Ti-6Al-4V in the $\alpha + \beta$ phase field.

5. Conclusions

The microstructure and microtexture evolution of an ELI grade Ti-6Al-4V alloy with a lamellar initial microstructure was investigated by means of isothermal compression tests over the temperature range $900\text{--}1050 \text{ }^\circ\text{C}$ and low strain rate range $10^{-3}\text{--}10^{-1} \text{ s}^{-1}$. The following conclusions were obtained from this study.

1. In the ranges 900–950 °C and 10^{-3} – 10^{-2} s⁻¹, globularization of the lamellar structure occurred. The process of globularization could be considered as a type of CDRX, and grain boundaries were formed by β penetrating the α platelets by diffusion. After globularization, the initial α {0001} texture softened, and the {0001} texture rotated to the TD direction. The globularization process resulted in texture randomization and the increasing strain rate led to more randomization.
2. In the ranges 900–950 °C and 10^{-2} – 10^{-1} s⁻¹, flow instabilities occurred; the instability mechanism was mainly flow localization, even cracking.
3. In the β range, DRX occurred at a temperature of 1050 °C and a strain rate of 10^{-3} s⁻¹.

Acknowledgments: The authors are grateful for the financial support provided by the National Nature Science Foundation of China. (Grant Nos. U1302275 and 51305304).

Author Contributions: Zhixiong Zhang and Shoujiang Qu conceived and designed the experiments; Zhixiong Zhang performed the experiments; Zhixiong Zhang and Xin Hu analyzed the data; Zhixiong Zhang and Aihan Feng and Jun Shen wrote the paper.

Conflicts of Interest: The authors declare no conflict of interest.

References

1. Xu, W.; Lui, E.W.; Pateras, A.; Qian, W.; Brandt, M. In situ tailoring microstructure in additively manufactured Ti–6Al–4V for superior mechanical performance. *Acta Mater.* **2017**, *125*, 390–400. [[CrossRef](#)]
2. Zhang, Z.X.; Qu, S.J.; Feng, A.H.; Shen, J. Achieving grain refinement and enhanced mechanical properties in Ti–6Al–4V alloy produced by multidirectional isothermal forging. *Mater. Sci. Eng. A* **2017**, *692*, 127–138. [[CrossRef](#)]
3. Li, B.; Shen, Y.; Luo, L.; Hu, W. Effects of processing variables and heat treatments on Al/Ti–6Al–4V interface microstructure of bimetal clad-plate fabricated via a novel route employing friction stir lap welding. *J. Alloy. Compd.* **2016**, *658*, 904–913. [[CrossRef](#)]
4. Boyer, R.; Welsch, G.; Collings, E.W. (Eds.) *Materials Properties Handbook: Titanium Alloys*; ASM International: Materials Park, OH, USA, 1994.
5. Prasad, Y.V.; Seshacharyulu, T.; Medeiros, S.C.; Frazier, W.G. A study of beta processing of Ti–6Al–4V: Is it trivial? *J. Eng. Mater. Technol.* **2001**, *123*, 355–360. [[CrossRef](#)]
6. Prasad, Y.V.; Seshacharyulu, T.; Medeiros, S.C.; Frazier, W.G. Microstructural modeling and process control during hot working of commercial Ti–6Al–4V: Response of lamellar and equiaxed starting microstructures. *Mater. Manuf. Process.* **2000**, *15*, 581–604. [[CrossRef](#)]
7. Seshacharyulu, T.; Medeiros, S.C.; Frazier, W.G.; Prasad, Y.V. Unstable flow during supratransus working of Ti–6Al–4V. *Mater. Lett.* **2001**, *47*, 133–139. [[CrossRef](#)]
8. Seshacharyulu, T.; Medeiros, S.C.; Morgan, J.T.; Malas, J.C.; Frazier, W.G.; Prasad, Y.V. Hot deformation and microstructural damage mechanisms in extra-low interstitial (ELI) grade Ti–6Al–4V. *Mater. Sci. Eng. A* **2000**, *279*, 289–299. [[CrossRef](#)]
9. Ding, R.; Guo, Z.; Wilson, A. Microstructural evolution of a Ti–6Al–4V alloy during thermomechanical processing. *Mater. Sci. Eng. A* **2002**, *327*, 233–245. [[CrossRef](#)]
10. Seshacharyulu, T.; Medeiros, S.C.; Frazier, W.G.; Prasad, Y.V. Microstructural mechanisms during hot working of commercial grade Ti–6Al–4V with lamellar starting structure. *Mater. Sci. Eng. A* **2002**, *325*, 112–125. [[CrossRef](#)]
11. Zhang, Z.X.; Qu, S.J.; Feng, A.H.; Shen, J.; Chen, D.L. Hot deformation behavior of Ti–6Al–4V alloy: Effect of initial microstructure. *J. Alloy. Compd.* **2017**, *718*, 170–181. [[CrossRef](#)]
12. Salem, A.A.; Semiati, S.L. Anisotropy of the hot plastic deformation of Ti–6Al–4V single-colony samples. *Mater. Sci. Eng. A* **2009**, *508*, 114–120. [[CrossRef](#)]
13. Lütjering, G. Influence of processing on microstructure and mechanical properties of (α + β) titanium alloys. *Mater. Sci. Eng. A* **1998**, *243*, 32–45. [[CrossRef](#)]
14. Semiati, S.L.; Seetharaman, V.; Weiss, I. The thermomechanical processing of alpha/beta titanium alloys. *JOM* **1997**, *49*, 33–39. [[CrossRef](#)]

15. Bhattacharyya, D.; Viswanathan, G.B.; Denkenberger, R.; Furrer, D.; Fraser, H.L. The role of crystallographic and geometrical relationships between α and β phases in an α/β titanium alloy. *Acta Mater.* **2003**, *51*, 4679–4691. [[CrossRef](#)]
16. Stanford, N.; Bate, P.S. Crystallographic variant selection in Ti–6Al–4V. *Acta Mater.* **2004**, *52*, 5215–5224. [[CrossRef](#)]
17. Stefansson, N.; Semiatin, S.L.; Eylon, D. The kinetics of static globularization of Ti–6Al–4V. *Metall. Mater. Trans. A* **2002**, *33*, 3527–3534. [[CrossRef](#)]
18. Semiatin, S.L.; Brown, J.O.; Brown, T.M.; DeLo, D.P.; Bieler, T.R.; Beynon, J.H. Strain-path effects during hot working of Ti–6Al–4V with a colony-alpha microstructure. *Metall. Mater. Trans. A* **2001**, *32*, 1556–1559. [[CrossRef](#)]
19. Semiatin, S.L.; Stefansson, N.; Doherty, R.D. Prediction of the kinetics of static globularization of Ti–6Al–4V. *Metall. Mater. Trans. A* **2005**, *36*, 1372–1376. [[CrossRef](#)]
20. Stefansson, N.; Semiatin, S.L. Mechanisms of globularization of Ti–6Al–4V during static heat treatment. *Metall. Mater. Trans. A* **2003**, *34*, 691–698. [[CrossRef](#)]
21. Weiss, I.; Froes, F.H.; Eylon, D.; Welsch, G.E. Modification of alpha morphology in Ti–6Al–4V by thermalmechanical processing. *Metall. Trans. A* **1986**, *17A*, 1935–1947. [[CrossRef](#)]
22. Seshacharyulu, T.; Medeiros, S.C.; Morgan, J.T.; Malas, J.C.; Frazier, W.G.; Prasad, Y.V. Hot deformation mechanisms in ELI grade Ti–6Al–4V. *Scr. Mater.* **1999**, *41*, 283–288. [[CrossRef](#)]
23. Zherebtsov, S.; Murzinova, M.; Salishchev, G.; Semiatin, S.L. Spheroidization of the lamellar microstructure in Ti–6Al–4V alloy during warm deformation and annealing. *Acta Mater.* **2011**, *59*, 4138–4150. [[CrossRef](#)]
24. Zherebtsov, S.; Mazur, A.; Salishchev, G.; Lojkowski, W. Effect of hydrostatic extrusion at 600–700 °C on the structure and properties of Ti–6Al–4V alloy. *Mater. Sci. Eng. A* **2008**, *485*, 39–45. [[CrossRef](#)]
25. Zherebtsov, S.V.; Salishchev, G.A.; Galeev, R.M.; Valiakhmetov, O.R.; Mironov, S.Y.; Semiatin, S.L. Production of submicrocrystalline structure in large-scale Ti–6Al–4V billet by warm severe deformation processing. *Scr. Mater.* **2004**, *51*, 1147–1151. [[CrossRef](#)]
26. Mironov, S.; Murzinova, M.; Zherebtsov, S.; Salishchev, G.A.; Semiatin, S.L. Microstructure evolution during warm working of Ti–6Al–4V with a colony- α microstructure. *Acta Mater.* **2009**, *57*, 2470–2481. [[CrossRef](#)]



© 2018 by the authors. Licensee MDPI, Basel, Switzerland. This article is an open access article distributed under the terms and conditions of the Creative Commons Attribution (CC BY) license (<http://creativecommons.org/licenses/by/4.0/>).